Results in Physics 6 (2016) 675–682

Contents lists available at ScienceDirect

Results in Physics

journal homepage: www.journals.elsevier.com/results-in-physics

Investigating the effect of Cd-Mn co-doped nano-sized $BiFeO_3$ on its physical properties

B. Ishaq [a], G. Murtaza [a,*], S. Sharif [b], M. Azhar Khan [c], Naeem Akhtar [d], I.G. Will [e], Murtaza Saleem [f], Shahid M. Ramay [g]

[a] Centre for Advanced Studies in Physics, GC University, Lahore 5400, Pakistan
[b] Department of Physics, GC University, Lahore 54000, Pakistan
[c] Department of Physics, Islamia University, Bahawalpur, Pakistan
[d] Department of Physics, Khawaja Fareed Government Postgraduate College, Rahim Yar Khan, Pakistan
[e] Spintronics Laboratory, Department of Electronics, The University of York, York YO10 5DD, UK
[f] Department of Physics, Lahore University of Management Sciences, Pakistan
[g] Department of Physics and Astronomy, College of Science, King Saud University, Riyadh, Saudi Arabia

ARTICLE INFO

Article history:
Received 3 August 2016
Received in revised form 24 August 2016
Accepted 28 September 2016
Available online 3 October 2016

Keywords:
Nanoparticles
Cd-Mn doped $BiFeO_3$
FESEM
XANES
Magnetic properties

ABSTRACT

This work deals with the investigation of different effects on the structural, magnetic, electronic and dielectric properties of Cd and Mn doped $Bi_{0.75}Cd_{0.25}Fe_{1-x}Mn_xO_3$ multiferroic samples by taking fixed ratios of Cd and varying the Mn ratio with values of x = 0.0, 0.5, 0.10 and 0.15. Cd-Mn doped samples were synthesized chemically using a microemulsion method. All the samples were finally sintered at 700 °C for 2 h to obtain the single phase perovskites structure of $BiFeO_3$ materials. The synthesized samples were characterized by different techniques, such as X-ray diffractometry (XRD), Scanning Electron Microscopy (SEM), Fourier transform infrared spectroscopy (FTIR), LCR meter and magnetic properties using VSM. XRD results confirm BFO is a perovskite structure having crystallite size in the range of 24–54 nm. XRD results also reveal observed structural distortion due to doping of Cd at the A-site and Mn at the B-site of BFO. SEM results depict that, as the substitution of Cd-Mn increases in BFO, grain size decreases up to 30 *nm*. FTIR spectra showed prominent absorption bands at 555 cm^{-1} and 445 cm^{-1} corresponding to the stretching vibrations of the metal ions complexes at site A and site B, respectively. Variation of dielectric constant (ε') and loss tangent (tan δ) at room temperature in the range of 1 MHz to 3 GHz have been investigated. Results reveal that with Cd-Mn co doping a slight decrease in dielectric constant have been observed. Magnetic properties of Cd-Mn doped pure BFO samples have been studied at 300 K. Results reveal that undoped $BiFeO_3$ exhibits weak ferromagnetic ordering due to the canting of its spin. Increase in magnetization and decrease in coercivity is a clear indication that a material can be used in high density recording media and memory devices.

Introduction

Multiferrioc materials exhibit ferroelectric, ferromagnetic and ferroelastic properties simultaneously. Due to strong coupling in electric and magnetic parameters, these materials have potential applications in spintronics, non-volatile memory devices, actuators and sensors. Multiferrioc such as, $BiFeO_3$ (BFO) attract much attention due their ferroelectricity (T_C = 826–845 °C) and G-type antiferromagnetism (T_N = 370 °C) at room temperature [1]. BFO is a perovskite oxide, offering rhombohedral symmetry with space group *R3c* along with the rhombohedral lattice parameters a_r = 5.63 Å = 5.63 Å, $\alpha_r = 59.35^0$, or alternatively, hexagonal parameters a_{hex} = 5.58 Å, c_{hex} = 13.87 Å [2,3]. Multiferroic studies reveal that $BiFeO_3$ is the only single phase material which possesses dual nature, i.e., magnetic and ferroelectric order at and above room temperature. Research on perovskite $BiFeO_3$ compounds initially flourished in the late 1950s [4], and the early studies have their roots in the important topic, magnetoelectric coupling [5]. It was also reported during the 1960s and 1970s that the true physical and structural properties of $BiFeO_3$ were not clear. However, a few studies revealed, in the early 1960s, its dual nature, i.e., an antiferromagnetic and ferroelectric multiferroic material [6,7]. The macroscopic scale modulated spiral spin structure of $BiFeO_3$ along $[1\ 1\ 0]_H$ with wave- length λ = 62 *nm* shows zero magnetization [8]. This leads to one of the main limitations that restrict its

* Corresponding author.
E-mail address: gmrai@gcu.edu.pk (G. Murtaza).

http://dx.doi.org/10.1016/j.rinp.2016.09.018
2211-3797/

applications in high temperature devices. Furthermore, the synthesis process may cause the loss of bismuth content, which is responsible for the generation of oxygen vacancies and valence fluctuation of Fe atoms which eventually produces a high leakage current in $BiFeO_3$ compounds [9]. To reduce the leakage current, site-engineering and the route of synthesis choices are important. Many studies reported that in BFO the substitution of A- or B-sites with the transition metal ions (Co, Ru, Cr, Ti, Mn, Zn etc.,) can enhanced the magnetoelectric properties [10–14]. Recent Investigation shows that magnetic properties are enhanced by suppressing the spiral spin structure of BFO and consequently enhances the multiferroic properties, by reducing the grain size. Usually, particle size also effects properties such as, magnetization and the magnetoelectric effects, these properties enhance as the particles size decreases below the periodicity of the order of the cycloid spin order [15–17].

Due to the decrease of particle size, cycloid spin order suppresses the cycloid structure, which is due to large crystalline strain present in the nanoparticles. In addition, the decreasing trend of particle size is responsible for the increases of magnetization of BFO samples, known as the finite-size effect [18]. We have investigated the Cd and Mn co-substituted effect in $BiFeO_3$. To the best of our knowledge, the effect of Cd at the A-site and Mn at B-site have been studied for the first time at nanoscale in this present work. In this study, four different types of samples were synthesized and analyzed:

1) BFO (without doping $BiFeO_3$).
2) Cd-doped BCFO ($Bi_{0.75}Cd_{0.25}FeO_3$).
3) Mn doped BCFO ($Bi_{0.75}Cd_{0.25}Fe_{1-x}Mn_xO_3$ with x = 0.05, 0.10 and 0.15).
4) BFO with 5% Mn ($BiFe_{0.95}Mn_{0.05}O$).

Variation of structural, surface morphology, electronic and dielectric properties of undoped (and different concentration of Cd-Mn) have been presented and discussed.

Experiment

The nanoparticles of undoped $BiFeO_3$ and Cd-Mn doped $Bi_{0.75}Cd_{0.25}Fe_{1-x}Mn_xO_3$ (with x = 0.0, 0.05, 0.10 and 0.15) have been synthesized using micro-emulsion technique. Analytical grade precursors such as $Bi(NO_3)_3$, $Fe(NO_3)_2{\cdot}4H_2O$, $Cd(NO_3)_2{\cdot}4H_2O$, $MnCl_2{\cdot}4H_2O$, CTAB (surfactant), NH_3 (Precipitating agent), methanol (washing agent) were used as starting materials. The solutions in stoichiometric proportions (1:1 M ratio) were mixed to obtain the metal nitrate solution in deionized water. The resulting solution was continuously stirred on a magnetic hot plate at 50–60 °C for 20–25 min. Aqueous ammonia solution was slowly dropped into the nitrate solution to maintain pH∼11 until the required precipitates formed. The resulting precipitates were finally washed several times using deionized water to reduce the pH up to neutral level ∼7 [19]. These precipitates were dried in a controlled muffle furnace at about 100 °C for 5 h and then sintered at 700 °C for 2 h to promote the crystallization of the prepared samples. The fine powders were prepared for characterization including X-ray diffraction (Philips using *Cu* Kα radiation) for structural information, Scanning Electron Microscope (model NOVA NanoSEM 200) for surface morphology, Fourier Transformation Infrared Spectroscopy (IR Prestige-21 Szhamdzu) for chemical analysis. Similarly, near edge X-ray Absorption Fine structure (NEXAFS) Spectroscopy for the determination of the oxidation state and their bonding. The latter were performed at the 1D KIST-PAL beamline in the 2.5-GeV Pohang light source (ring current of 120–160 mA).

Results and discussion

Structure analysis

X-ray diffraction patterns were taken at room temperature and are given in Fig. 1. The standard pattern (ICSD 01-071-2494) was used to analyzed spectra and the results reveal that the pure BFO and Mn doped BFO samples have typical perovskites structures [20]. However, a few peaks of $Bi_2Fe_4O_9$ as secondary phases have been identified using card number (020-0836). The pure BFO and Mn doped BFO samples are very similar to each other. However, slight variations in the peaks are identified in the Mn doped BCFO, as compared to undoped BFO and BCFO samples. It can be seen from Fig. 1 that with the substitution of Cd ions at the Bi sites, the peaks are shifted toward the higher angle. It is clear evidence for the incorporation of Cd ions having ionic radii 0.87 A, which is lower than the Bi ionic radii 0.96 A. The calculated lattice parameters *a* and *c* given in Table 1 decrease due to the lesser ionic radii contents, which causes the stress in the crystal structure. XRD results also reveal that, due to Cd-Mn co doping, peaks broaden and crystallites size measured by the sherrer equation decreases. The presence of Mn with Cd can also be analyzed by the behavior of the main peaks in the spectra, in the 5% and 10% Mn content (1 0 4) the peak disappear, whilst for 15% Mn concentration they re-appear in the spectra. It can be observed that 5% Mn concentration with Cd is the optimum value to obtain lower crystallite size, whilst having good crystalline samples [21–23].

Surface morphology

The size of the particles and surface morphology of all the samples have been investigated by SEM and presented in Fig. 2(a–f) and given in Table 2. The SEM images establish the effects of Cd-Mn co doped in BFO multiferroic materials. It is observed that the size decreases with Cd substitution as for sample BCFO shown in Fig. 2(a). Whereas, Cd-Mn co doped increases the trend of decreasing particle size. Furthermore, this decreasing trend is enough for the 5% concentration of Mn, which is well agreement with XRD results. However, due to smaller size of the particles, agglomeration has been observed i.e. the nanoparticles are agglomerated and there is a high interconnection between grains [24], which can be seen in Fig. 2(a–f).

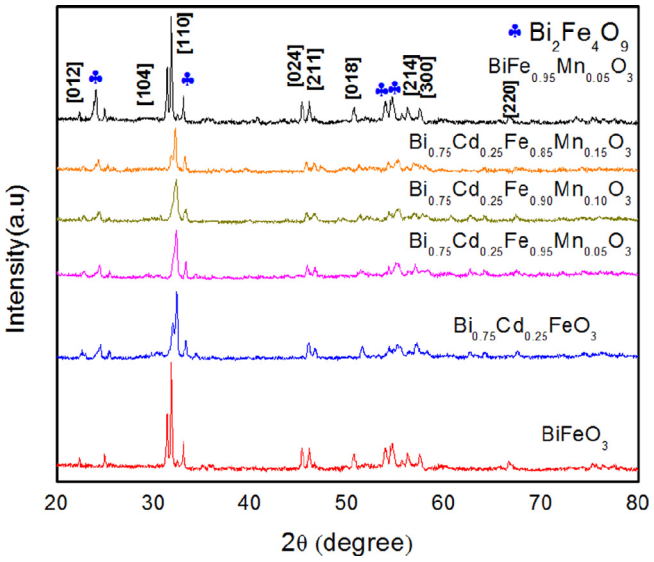

Fig. 1. XRD Spectra of multiferroic materials $BiFeO_3$, B $i_{0.75}Cd_{0.25}Fe_{1-x}Mn_xO_3$ (x = 0.0, 0.5, 0.10 and 0.15), $BiFe_{0.95}Mn_{0.05}O_3$.

Table 1
Lattice parameters (a, b, c), cell volume and crystalline size calculated by XRD.

Composition	a (Å)	b (Å)	c (Å)	Cell volume (Å^3)	Crystallite size
$BiFeO_3$	3.648	4.413	18.206	209.82	53.6
$Bi_{0.75}Cd_{0.25}FeO_3$	3.62	4.278	19.742	224.04	30.0
$Bi_{0.75}Cd_{0.25}Fe_{0.95}Mn_{0.05}O_3$	3.646	4.245	19.660	226.33	34.9
$Bi_{0.75}Cd_{0.25}Fe_{0.90}Mn_{0.10}O_3$	3.652	4.242	19.784	228.50	23.7
$Bi_{0.75}Cd_{0.25}Fe_{0.85}Mn_{0.15}O_3$	3.655	4.257	19.949	230.79	36.2
$BiFe_{0.95}Mn_{0.05}O_3$	3.655	4.437	18.504	214.07	53.7

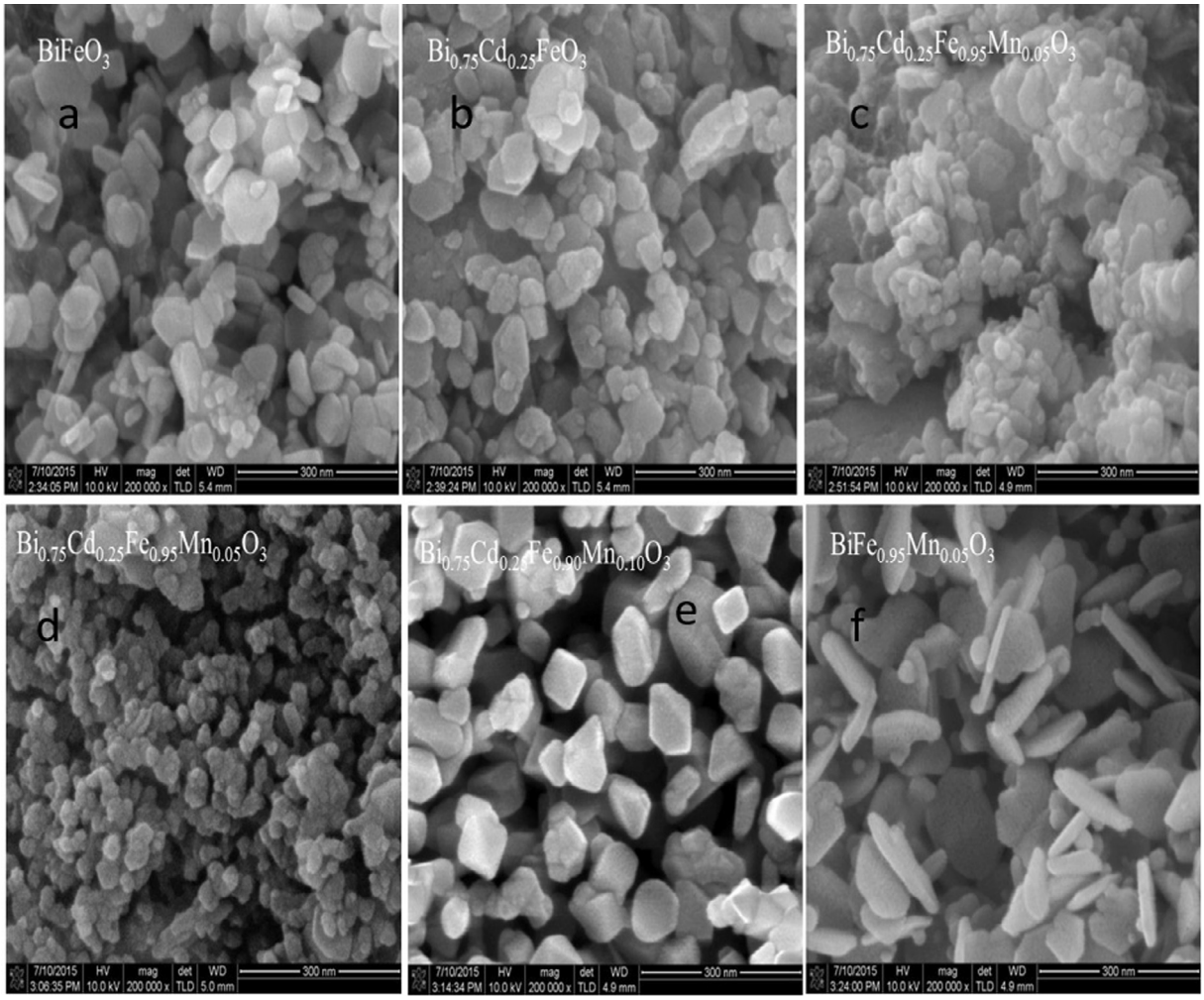

Fig. 2. SEM images (a–f) of $BiFeO_3$, $Bi_{0.75}Cd_{0.25}Fe_{1-x}Mn_xO_3$ (x = 0.0, 0.5, 0.10 and 0.15), $BiFe_{0.95}Mn_{0.05}O_3$.

Table 2
Average grain size measured by linear intercept method of Multiferroic different BFO samples.

Elements	Size of particle (nm)
$BiFeO_3$	86.3
$Bi_{0.75}Cd_{0.25}FeO_3$	50.3
$Bi_{0.75}Cd_{0.25}Fe_{0.95}Mn_{0.05}O_3$	54.2
$Bi_{0.75}Cd_{0.25}Fe_{0.90}Mn_{0.10}O_3$	37.8
$Bi_{0.75}Cd_{0.25}Fe_{0.85}Mn_{0.15}O_3$	58.8
$BiFe_{0.95}Mn_{0.05}O_3$	87.7

Near edge X-ray absorption fine structure (NEXAFS) spectroscopy

The XANES provides information on the oxidation state of the absorbing element as a function of photon energy. XANES also helpful to get information regarding unoccupied DOS, phase transition, local symmetry, as well as lattice strain [25].

I. **Bi $N_{5,4}$-edge.** Analysis of the spectrum for Bi $N_{5,4}$-edge as shown in Fig. 5(a), reveals the changes after doping of Cd and Mn in BFO in local environment. Two N_5 and N_4 edges of Bi arise at different energies. The peaks at these regions are due to the transition of Bi $2p_{3/2}$ and $2p_{1/3}$ levels to the 3d unoccupied state. Results show that no significant variation in the intensity and shifting of peaks have been observed, which is clearly evidence about the stability of Bi^{3+} oxidation sate after doping of Cd and Mn ions.
II. **Cd $M_{5,4}$-edge.** Fig. 5(b) shows the $M_{4,5}$ edge spectra of Cd ions, having two regions M_5 and M_4 at 401 eV, 408 eV respectively. These regions are due to transition of Cd $3d_{5/2}\rightarrow$ 4f and $3d_{3/2}\rightarrow$ 4f levels. Results reveal that there is

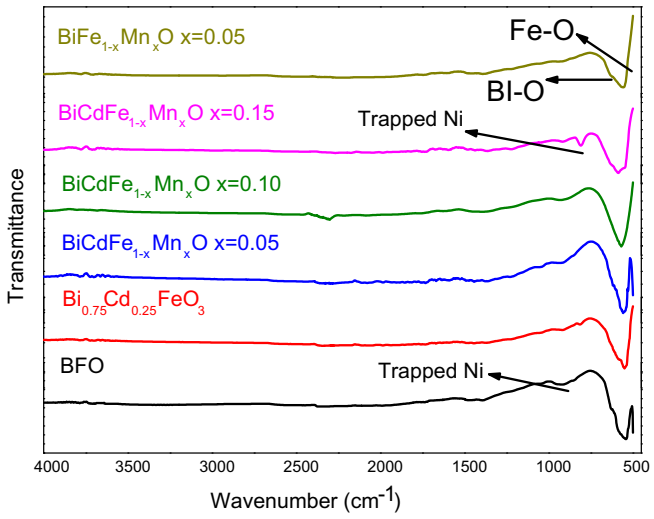

Fig. 3. FTIR Spectra of multiferroic materials $BiFeO_3$, $Bi_{0.75}Cd_{0.25}Fe_{1-x}Mn_xO_3$ (x = 0.0, 0.5, 0.10 and 0.15), $BiFe_{0.95}Mn_{0.05}O_3$.

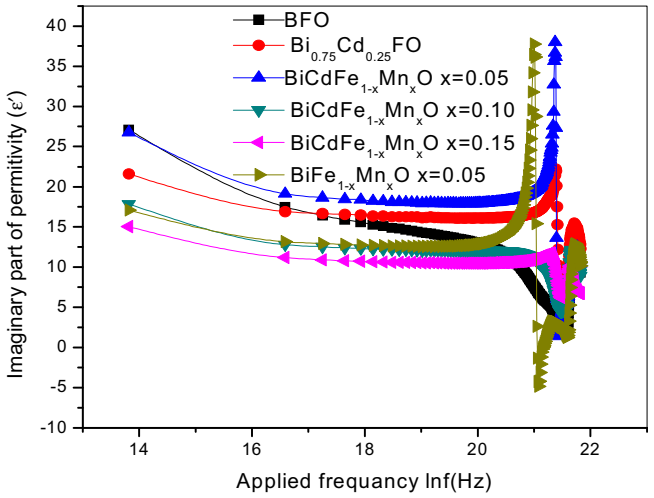

Fig. 4a. Frequency dependent dielectric constant (ε′) of $BiFeO_3$, $Bi_{0.75}Cd_{0.25}Fe_{1-x}Mn_xO_3$ (x = 0.0, 0.5, 0.10 and 0.15), $BiFe_{0.95}Mn_{0.05}O_3$ Multiferroics.

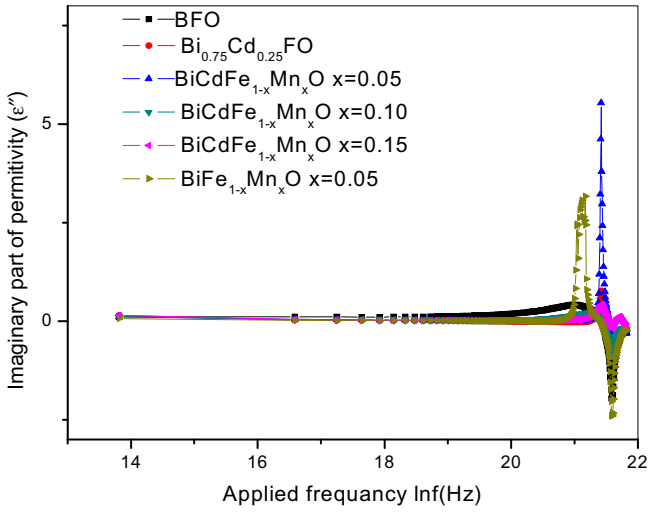

Fig. 4b. In frequency dependent of the dielectric dissipation factor (ε″) of $BiFeO_3$, $Bi_{0.75}Cd_{0.25}Fe_{1-x}Mn_xO_3$ (x = 0.0, 0.5, 0.10 and 0.15), $BiFe_{0.95}Mn_{0.05}O_3$ Multiferroics.

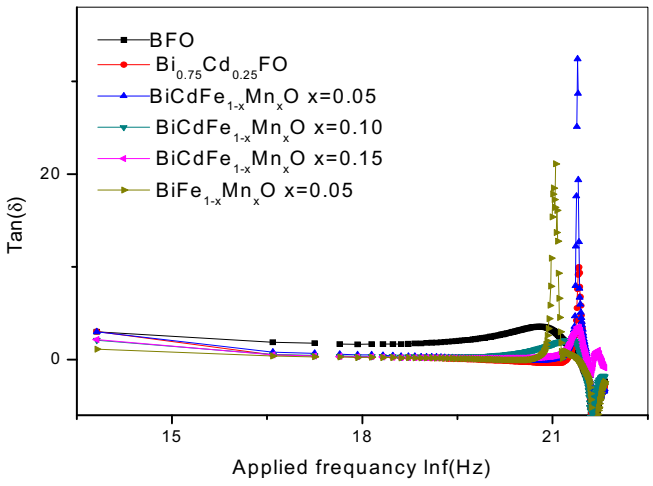

Fig. 4c. Frequency dependent tangent loss factor (Tan δ) of $BiFeO_3$, $Bi_{0.75}Cd_{0.25}Fe_{1-x}Mn_xO_3$ (x = 0.0, 0.5, 0.10 and 0.15), $BiFe_{0.95}Mn_{0.05}O_3$ Multiferroics.

no shift in the shape of M_4 and M_5 due to the substitution of Cd into Bi ions. Furthermore, variation observed in the spectra shows no change in the oxidation state of the cadmium either.

III. **Fe $L_{3,2}$-edge.** The discussion regarding the spectrum of Fe *L*-edge XANES as given in Fig. 5(c) is based upon two regions, firstly the pre-edge L_3- and secondly, the post edge L_2-. It has been analyzed that the peaks in these two regions are due to the transitions of electrons to bound excited electronic states and continuum states, respectively. Results also reveal that there are two main peaks belonging to the L_3- and L_2-edges at ~711.8 eV and ~724.8 eV, which arises due to electronic transitions of the Fe $2p_{3/2}$ and $2p_{1/2}$ core electrons. Furthermore, the existence of these peaks is associated with the split by the spin-orbit interaction of the Fe 2p core level, to an unoccupied 3d level highly hybridized with an oxygen 2p orbital, respectively, as shown in Fig. 5(c). Basically, the dipole selection rule explains the hybridization of iron 2p characterised by a sharp, highly structured transition-metal 3d band [26]. Results indicate that the pre-edge peak (1s-3d), which gives the most useful feature to discriminate between oxidation states [27,28], has no shift in its peaks. Therefore, doping does not change the oxidation state of the Fe^{3+}-Fe^{2+} ions in all the samples.

IV. **Mn $L_{3,2}$-edge.** Fig. 5(d) depicts the spectra of the Mn $L_{3,2}$-edge, having two regions of Mn. L_3(640 eV) and L_2(651 eV) respectively. These peaks are due to the transition of Mn $2p_{3/2}\rightarrow$ 3d and $2p_{1/2}\rightarrow$ 3d and present two groups of multiplets separated by the spin-orbit interaction of the Mn 2*p* core hole. Results reveal that there is no spectral change in the spectra, which indicates that the oxidation state remains same due to chemical substitution of Mn ions into Fe sites.

V. **K-edge.** The spectra of O *K*-edge structure, as shown in Fig. 5(e), reveals two regions: the pre-edge and post-edge [29]. It is said that the pre-edge is the low-energy region between the absorption threshold and the absorption jump, and the post-edge region extends to about 50 eV past the continuum threshold [30]. This arises due to transition of electrons from $2p_{3/2}$ and $2p_{1/3}$ levels to the 3d electronic states and continuum states, respectively, as near the threshold, the oxygen 2p character is hybridized with the more sharply defined transition-metal 3d band. While in the second region, the 2p band of oxygen hybridized weakly

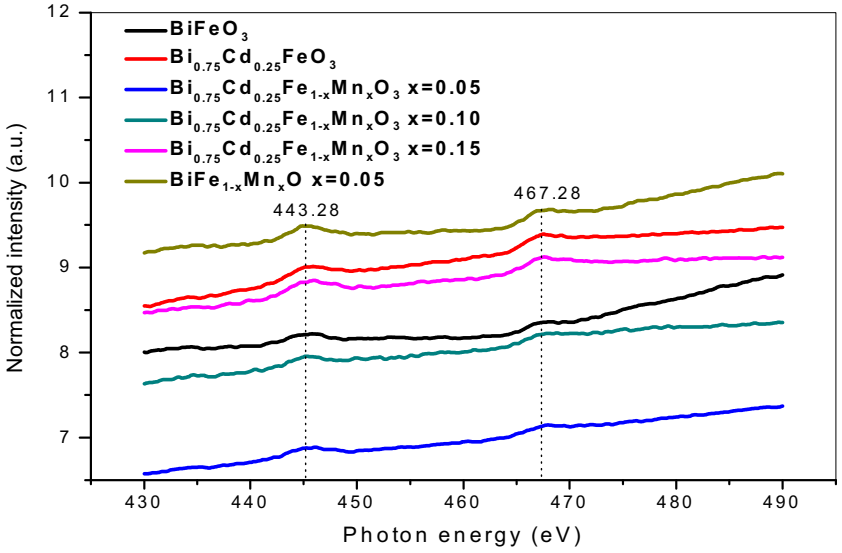

Fig. 5a. XANES Spectra of $N_{4,5}$ edge of Bi multiferroic materials $BiFeO_3$, $Bi_{0.75}Cd_{0.25}Fe_{1-x}Mn_xO_3$ (x = 0.0, 0.5, 0.10 and 0.15), $BiFe_{0.95}Mn_{0.05}O_3$.

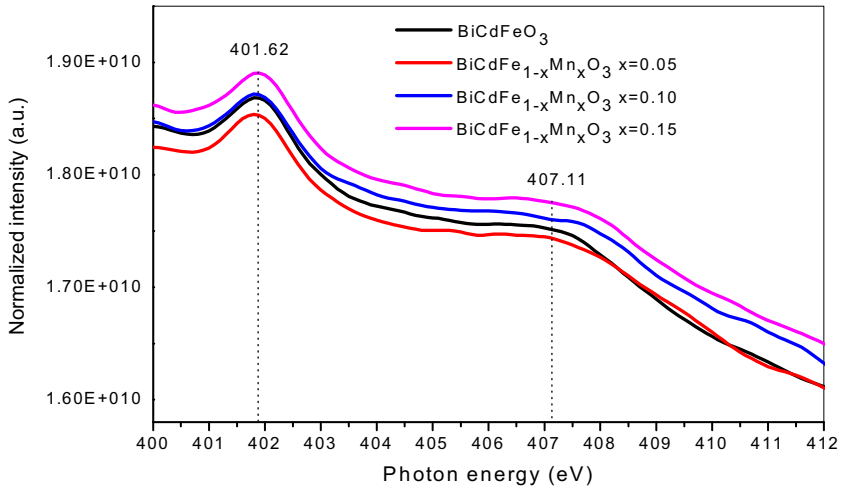

Fig. 5b. XANES Spectra of $M_{4,5}$ edge of Cd multiferroic materials $Bi_{0.75}Cd_{0.25}Fe_{1-x}Mn_xO_3$ (x = 0.0, 0.5, 0.10 and 0.15).

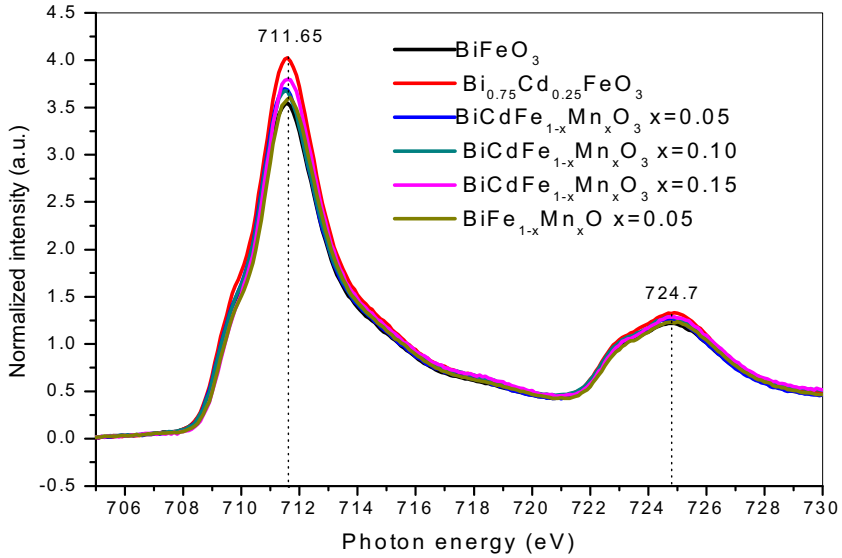

Fig. 5c. XANES Spectra of $L_{3,2}$ edge of Fe multiferroic materials $Bi_{0.75}Cd_{0.25}Fe_{1-x}Mn_xO_3$ (x = 0.0, 0.5, 0.10 and 0.15), $BiFe_{0.95}Mn_{0.05}O_3$.

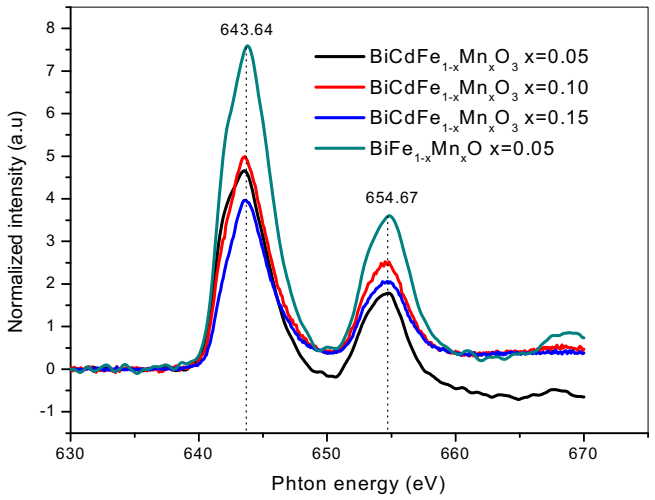

Fig. 5d. XANES Spectra of $L_{3,2}$ edge of Mn multiferroic materials $Bi_{0.75}Cd_{0.25}Fe_{1-x}Mn_xO_3$ (x = 0.0, 0.5, 0.10 and 0.15), $BiFe_{0.95}Mn_{0.05}O_3$.

with 4sp band. Results reveal that the integrated intensity of the 4sp region is at least equal to that of the 3d band region, which is indicative of the significance and contribution of metal 4sp states to the covalent nature of the transition-metal oxides. It is clearly observed that there is no change in the shape of edge, which is the evidence for the oxidation state remaining stable in all the samples of BFO.

FTIR analysis

The FT-IR spectrum of BFO, BCFO, BCMFO and BMFO samples are shown in the Fig. 3. The results show that in perovskite structure strong bands appear at 555 cm^{-1} and 445 cm^{-1} in the annealed powder. These absorption bands at 555 cm^{-1} and 445 cm^{-1} are associated with the O-Fe-O stretching and bending vibrations. This is characteristic of FeO_6 octahedral in the perovskite structure [31]. The perovskite structure can be confirmed by the metal-oxygen absorption band [32,33]. Absorption bands in the range of 424 cm^{-1} to 544 cm^{-1} are assigned with Bi-O vibrations. FTIR spectrum in the range between 500 and 4000 cm^{-1} provides much information about the structure and bonding between molecules. FTIR spectra shows absorption bands above 1250 cm^{-1} is due to moisture in samples. In these samples there is no absorption spectrum above 1250 cm^{-1}, which shows that there is no moisture in these samples. Samples were completely dry [34]. An FTIR spectral bands appear at 1300 cm^{-1} which is due to trapped nitrogen [35]. Bands appears at 761 cm^{-1}, 1085 cm^{-1} and 1150 cm^{-1} and are assigned to Mn-O vibrations [36]. The presence of Cd is confirmed by the FTIR spectrum in which bands are present in the range between 1270 cm^{-1} to 1641 cm^{-1} [37].

Dielectric properties

The dielectric constant is a measure of permittivity, or the effect of a material on applied electric field, or simply measure of the extent of polarization of a material. Dielectric constant of any material depends upon the method of synthesis, structure of material and composition of material. The effects of frequency on the dielectric constant for BFO are shown in Fig. 4. Dielectric constant of multiferroic material can be calculated by the Eq. (1).

$$\varepsilon' = \frac{Cd}{\varepsilon A} \tag{1}$$

where, C = capacitance of the pellet (Farad), A = cross sectional area of the flat surface of pellet, d = thickness of the pellet (meters), ε_o = constant of permeability.

The variation of the dielectric constants were determined in the frequency range from 1 MHz to 3 GHz. Results reveal that the higher value of the dielectric constant at lower frequency (100 Hz) may be explained in terms of a model based on barrier layer formation. It has been studied, using this model, that existence of interfacial space charge polarization is responsible for the formation of a barrier layer at the grain to grain boundary interfaces. Therefore, the Maxwell–Wagner type dielectric relaxation occurs in BFO, BCFO, BCMFO and BMFO due to semiconducting grains separated by an insulating grain boundary [38,39]. Orientation polarization forms as a result of the alignment of Fe^{3+}-Fe^{2+} dipoles in the direction of the applied electric field. It is observed that the dielectric constant decreases as applied electric field frequency increases and at higher frequencies fewer resonance peaks appeared. Dielectric constant decreases, because the orientation polarization cannot "keep up" with switching of the applied electric field and that is why dielectric constant becomes constant at higher frequencies [40]. After substitution of Cd^{3+} (0.97 Å) and Mn^{3+} (0.46 Å) with Bi^{3+} (1.03 Å) and Fe^{2+} (0.645 Å) respectively the dielectric constant decreases, in the sample of $BiFe_{1-x}Mn_xO_3$ where x = 0.05, the dielectric constant value is at a minimum. In all samples at lower frequencies the dielectric con-

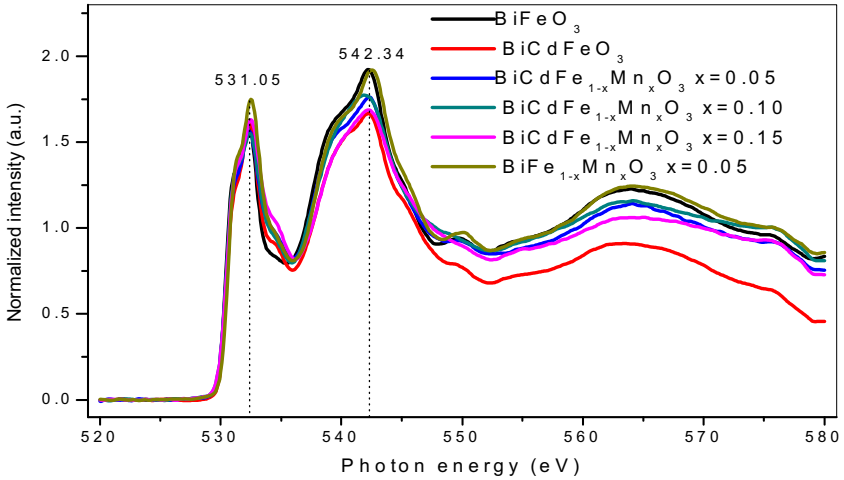

Fig. 5e. XANES Spectra of K edge of O multiferroic materials $BiFeO_3$, $Bi_{0.75}Cd_{0.25}Fe_{1-x}Mn_xO_3$ (x = 0.0, 0.5, 0.10 and 0.15), $BiFe_{0.95}Mn_{0.05}O_3$.

stant shows stability, but after a while, a few relaxation peaks appeared. This is due to the external applied AC electric field becoming equal to the jumping frequency of electric charge carriers, causing the relaxation peaks to appear. With the increasing concentration of substitution, the peaks shifted towards higher frequency. Fig. 4(b) show the dielectric loss factor ε'' of all the samples at room temperature. Results reveal that the dielectric loss, i.e., energy loss [41], is almost constant with respect to applied electric field frequency and at higher frequencies few resonance peaks appeared. Actually, the amount of energy dissipated in the dielectric decreases with increasing applied oscillating electric field frequency. At lower frequencies of applied oscillating electric field, energy dissipated in dielectric is high due to the resistivity of grain boundaries. Therefore, electrons need more energy for conversation between Fe^{3+} and Fe^{2+} ions due to high resistivity at lower frequencies. But, at high frequency the resistivity of the grain boundaries is much smaller than at lower frequency, and so electrons only need a small amount of energy for conversation between Fe^{3+} and Fe^{2+}. Hence, the movement of dipoles raises the temperature of the material, which is responsible for the dielectric dissipation. It is concluded that materials having low conductivity and high resistivity have low dielectric dissipation losses and the materials shows high conductivity and low resistivity having high dielectric losses [42]. Fig. 4(c) depicts the tangent loss of these samples, which is almost constant in the beginning at lower frequencies. In the beginning tangent loss is almost constant but at higher frequencies shows relaxation peaks due to the fact that electron between Fe^{3+} and Fe^{2+} do not follow the frequency of the applied field.

Magnetic properties

The magnetic properties of Cd-Mn doped $BiFeO_3$ have been investigated and the results are presented in Fig. 6; we have variety of samples, such as, BFO, BCFO, BCMFO and BMFO. The variation in results are also due to presence of different dopant at different concentration. Generally, the hysteresis loops depict the soft nature of each sample and the magnetic properties are given in Table 3. We can see that the magnetic properties of pure samples i.e., BFO show the weak ferromagnetic ordering having a coercivity field of 1900 Oe, and a magnetization of 0.509 emu/g. The results show that this weak ferromagnetism in pure BFO nanoparticles is due to the canting of spins [43]. It has been observed that with 25% doping of Cd in BFO, sample exhibit a lowering of the magnetization at room temperature. There are two reasons for the lowering in magnetization.

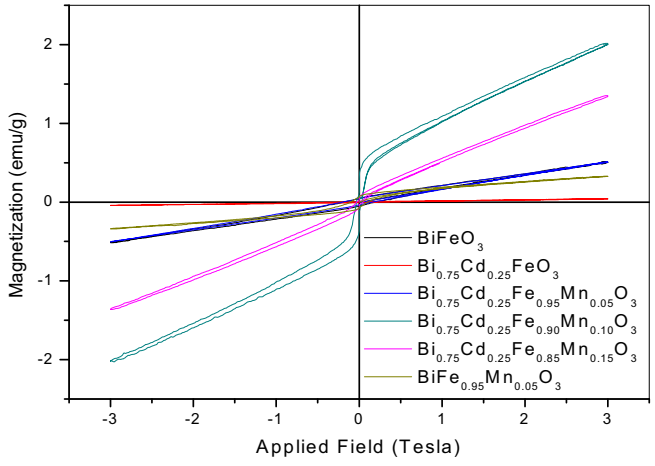

Fig. 6. Hysteresis loop curves for $BiFeO_3$, $Bi_{0.75}Cd_{0.25}Fe_{1-x}Mn_xO_3$ (x = 0.0, 0.5, 0.10 and 0.15), $BiFe_{0.95}Mn_{0.05}O_3$ nano-structure at room temperature.

Table 3
Various magnetic parameters of $BiFeO_3$, $Bi_{0.75}Cd_{0.25}Fe_{1-x}Mn_xO_3$ (x = 0.0, 0.5, 0.10 and 0.15), $BiFe_{0.95}Mn_{0.05}O_3$ nanoparticles.

Samples	Coercive field Hc (Oe)	Remnant magnetization Mr (emu/g)	Spontaneous magnetization Ms (emu/g)
$BiFeO_3$	1900	0.039	0.509
$Bi_{0.75}Cd_{0.25}FeO_3$	3200	0.006	0.040
$Bi_{0.75}Cd_{0.25}Fe_{0.95}Mn_{0.05}O_3$	2000	0.042	0.51
$Bi_{0.75}Cd_{0.25}Fe_{0.90}Mn_{0.10}O_3$	300	0.29	2.01
$Bi_{0.75}Cd_{0.25}Fe_{0.85}Mn_{0.15}O_3$	500	0.06	1.36
$BiFe_{0.95}Mn_{0.05}O_3$	1300	0.07	0.34

Firstly, structural distortion, due to Cd in BFO orthorhombic perovskite, can allow weak ferromagnetic ordering due to canting of the spins [44]. The magnetization of the pure samples has been calculated up to 0.039 emu/g, and decreases to 0.006 emu/g for 25% Cd doped BFO, while the coercivity increases up to 3200 Oe. Similarly, with Cd-Mn co doping coercivity decreases up to 500 Oe. The origin of magnetization is due to the nano-scale crystal size [45]. Doping of Cd-Mn increases the crystalline, whilst the grain size of samples decreases to some extent and then increase as confirmed by XRD and SEM analysis. The helical order in nanocrystal can be very suppressed by decreasing the particle size, which leads to higher magnetization in BFO [16]. When the doping of Cd and Mn increases further the crystalline size of samples increases which leds to a decrease in magnetization as presented in Table 3. Due to the doping of Cadmium and Manganese, remanence magnetization increases to some extent and then decreases. The increase in remanence is due to the suppressed magnetic spin structure. The decrease in remanent magnetization is due to the presence of a large amount of nonmagnetic Cadmium (Cd) ions which weakens the super exchange interaction. Secondly, after doping, the increase in magnetism is due to the distortion in the structure of the BFO. After doping, the structure of the BFO is distorted and is confirmed by XRD patterns of Cd-Mn doped BFO samples. BFO with a rhombohedral structure allows a weak ferromagnetic ordering due to the canting of spins [46].

Conclusion

Cd-Mn doped BFO samples have been synthesized by a simple chemical method known as the co-precipitation method and the effects of doping on structural, surface morphological and electrical properties have been investigated by different characterization techniques such as XRD, SEM, FTIR, and LCR. The following conclusions have been drawn as a result. XRD confirmed the rhombohedral structure of BFO having crystalline size in the range of 23 nm-54 nm. Surface morphology of Cd-Mn doped BFO samples are calculated by using SEM. SEM data tells us that the grain size is in the range of 37–86 nm. FTIR data confirms the O-Fe-O stretching and bending vibrational band at 555 cm^{-1} and 445 cm^{-1}, which indicates the presence of a perovskite structure. Absorption bands in the range from 450 cm^{-1} to 600 cm^{-1} confirm the presence of Bi-O, Mn^{3+}-O and Cd-O vibrations. The LCR meter investigated the dielectric constant of Cd-Mn doped BFO samples. The LCR meter data tells us that, by increasing the substitution of Cd-Mn in BFO, the dielectric constant of samples can reduce. After substitution, the value of the dielectric constant and tangent loss decreases to a minimum value. Both Cd and Mn are responsible for decreases in dielectric constant. These results shows decreases in the capacitance in the multi-layer chip components. Magnetic properties shows enhancement in magnetism which is very useful in industrial applications. Increase in magnetization and decreases in coercivity is a clear indication that the material can be used in high density recording media and memory devices.

Acknowledgement

The authors would like to extend sincere appreciation to the Deanship of Scientific Research at King Saud University for funding this Research Group (No. RG 1435-004).

References

[1] Chauhan S, Kumar M, Chhoker S, Katyal S, Jewariya M, Suma B, Kunte G. Ceram Int 2015;41:14306–14.
[2] Godara S, Kumar B. Ceram Int 2015;41:6912–9.
[3] Catalan G, Scott JF. Adv Mater 2009;21:2463–85.
[4] Royen P, Swars K. Angew Chem 1957;69. 779–779.
[5] Kubel F, Schmid H. Acta Crystallogr B 1990;46:698–702.
[6] Lakshmi KSRPVB, Ramachandran K. Cryst Res Technol 2008;44:153.
[7] Kiselev S, Ozerov R, Zhdanov G. Sov Phys Dokl 1963;7:742.
[8] Ruette B, Zvyagin S, Pyatakov A, Bush A, Li J, Belotelov V, Zvezdin A, Viehland D. Phys Rev B 2004;69:064114.
[9] Safi R, Shokrollahi H. Prog Solid State Chem 2012;40:6–15.
[10] Yan H, Deng H, Ding N, He J, Peng L, Sun L, Yang P, Chu J. Mater Lett 2013;111:123–5.
[11] Yang K, Zhang Y, Yang S, Wang B. J Appl Phys 2010;107:4109.
[12] Kubota M, Oka K, Yabuta H, Miura K, Azuma M. Inorg Chem 2013;52:10698–704.
[13] Singh V, Verma V, Ishigami K, Shibata G, Yamazaki Y, Fujimori A, Takeda Y, Okane T, Saitoh Y, Yamagami H. J Appl Phys 2013;114:103905.
[14] Azuma M, Kanda H, Belik AA, Shimakawa Y, Takano M. J Magn Magn Mater 2007;310:1177–9.
[15] Reddy VA, Pathak N, Nath R. J Alloy Compd 2012;543:206–12.
[16] Park T-J, Papaefthymiou GC, Viescas AJ, Moodenbaugh AR, Wong SS. Nano Lett 2007;7:766–72.
[17] Chaudhuri A, Mitra S, Mandal M, Mandal K. J Alloy Compd 2010;491:703–6.
[18] Batlle X, Labarta A. J Phys D Appl Phys 2002;35:R15.
[19] Soares-Carvalho F, Thomas P, Mercurio J, Frit B, Parola S. J Sol-Gel Sci Technol 1997;8:759–63.
[20] Jayakumar O, Achary S, Girija K, Tyagi A, Sudakar C, Lawes G, Naik R, Nisar J, Peng X, Ahuja R. Appl Phys Lett 2010;96:032903.
[21] Pell J, Delak K, Zur Loye H-C. Chem Mater 1998;10:1764–70.
[22] Galembeck A, Alves O. J Mater Sci 2002;37:1923–7.
[23] Chen C, Cheng J, Yu S, Che L, Meng Z. J Cryst Growth 2006;291:135–9.
[24] Bellakki M, Manivannan V. J Sol-Gel Sci Technol 2010;53:184–92.
[25] Unruan S, Srilomsak S, Priya S, Jantaratana P, Rujirawat S, Yimnirun R. Ceram Int 2015;41:4087–92.
[26] Abbate M, De Groot F, Fuggle J, Fujimori A, Strebel O, Lopez F, Domke M, Kaindl G, Sawatzky G, Takano M. Phys Rev B 1992;46:4511.
[27] Nedoseykina T, Kim MG, Park S-A, Kim H-S, Kim S-B, Cho J, Lee Y. Electrochim Acta 2010;55:8876–82.
[28] Berry AJ, O'Neill HSC, Jayasuriya KD, Campbell SJ, Foran GJ. Am Mineral 2003;88:967–77.
[29] De Groot F, Grioni M, Fuggle J, Ghijsen J, Sawatzky G, Petersen H. Phys Rev B 1989;40:5715.
[30] Chen JG. Surf Sci Rep 1997;30:1–152.
[31] Li S, Condrate Sr R, Jang S, Spriggs R. J Mater Sci 1989;24:3873–7.
[32] Yamaguchi O, Narai A, Komatsu T, Shimizu K. J Am Ceram Soc 1986;69:C-256–7.
[33] Palkar V, John J, Pinto R. Appl Phys Lett 2002;80:1628–30.
[34] Slamovich EB, Aksay IA. J Am Ceram Soc 1996;79:239–47.
[35] Nakagawa I, Walter J. J Chem Phys 1969;51:1389–97.
[36] Iakovlev S, Solterbeck C-H, Kuhnke M, Es-Souni M. J Appl Phys 2005;97:094901.
[37] Sakthivel S, Mangalaraj D. Nano Vision 2011;1:47–53.
[38] Dwivedi R, Kumar D, Parkash O. J Phys D Appl Phys 2000;33:88.
[39] Adams TB, Sinclair DC, West AR. Adv Mater 2002;14:1321–3.
[40] Singh N, Kumar P, Rai R. J Alloy Compd 2011;509:2957–63.
[41] Hussain T, Siddiqi SA, Atiq S, Awan M. Prog Nat Sci 2013;23:487–92.
[42] Kim A, Han S, Kang H-W, Lee H-G, Kim J, Cheon C. Ceram Int 2012;38: S397–401.
[43] Cheng Z, Wang X, Kannan CV, Ozawa K, Kimura H, Nishida T, et al. Appl Phys Lett 2006;88:132909.
[44] Cheng Z, Wang X. Phys Rev B 2007;75:172406.
[45] Chauhan S, Kumar M, Chhoker S, Katyal S, Singh H, Jewariya M, Yadav K. Solid State Commun 2012;152:525–9.
[46] Bellakki M, Manivannan V. J Mater Sci 2010;45:1137–42.